ACS APPLIED MATERIALS & INTERFACES

Research Article

www.acsami.org

Microwave-Assisted and Gram-Scale Synthesis of Ultrathin SnO_2 Nanosheets with Enhanced Lithium Storage Properties

Youqi Zhu, Huizi Guo, Huazhang Zhai,* and Chuanbao Cao*

Research Center of Materials Science, Beijing Institute of Technology, Beijing 100081, China

Supporting Information

ABSTRACT: The rational design and fabrication of SnO_2-based anode materials could offer a powerful way of effectively alleviating their large volume variation and guaranteeing excellent reaction kinetics for electrochemical lithium storage. Herein, we present an ultrarapid, low-cost, and simple microwave-assisted synthesis of ultrathin SnO_2 nanosheets at the gram-scale. The two-dimensional (2D) anisotropic growth depends on microwave dielectric irradiation coupled with surfactant structural direction, and is conducted under low-temperature atmospheric conditions. The ultrathin 2D nanostructure holds a great surface tin atom percentage with high activity, where the electrochemical reaction processes could be facilitated that highly dependent on the surface. Compared with 1D SnO_2 nanorods, the ultrathin SnO_2 nanosheets exhibit remarkably improved electrochemical lithium storage properties with a high reversible capacity of 757.6 mAh g^{-1} at a current density of 200 mA g^{-1} up to 40 cycles as well as excellent rate capability and cycling stability. Specifically, the ultrathin 2D nanosheet could significantly reduce ion diffusion paths, thus allowing faster phase transitions, while the sufficient external surface interspace and interior porous configuration could successfully accommodate the huge volume changes. Even more importantly, we develop a promising strategy to produce ultrathin SnO_2 nanosheets to tackle their intrinsic problems for commercial applications.

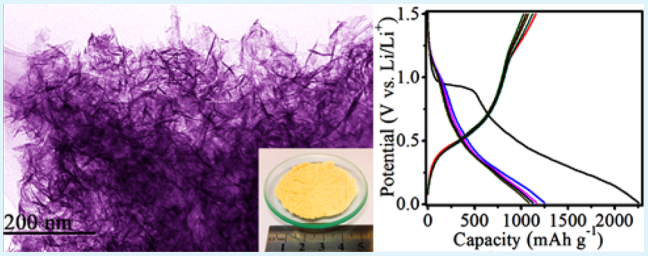

KEYWORDS: *two-dimensional nanostructure, SnO_2 nanosheet, microwave-assisted synthesis, anode, lithium ion battery*

1. INTRODUCTION

Due to its high theoretical specific capacity (782 mA h g^{-1}) and low lithium-ion intercalation potential, SnO_2 has been considered as one of the most promising substitutes for commercial graphite anodes for next-generation lithium ion batteries with high power and energy density.[1] The electrochemical lithium storage process of SnO_2-based anode materials is dependent on the Li−Sn alloying and dealloying mechanism.[2] During electrochemical operation, the SnO_2 anodes inevitably undergo huge volume variation (~300%) due to the repeated expansion and contraction of the converted tin lattice.[3] Consequently, these large volume changes can cause mechanical strain, leading to fatigue failure of the electrochemical active materials and structural disintegration of the electrodes.[2,4] This so-called pulverization could bring about mechanical fracture and a breakdown in electrical contact pathways between adjacent active Sn particles and conductive additives or current collector.[5−10] The above-mentioned issue could induce rapid deterioration and low retention of capacity upon extended cycling, thus hindering the practical application of SnO_2 anode materials. Therefore, it is highly desirable to address the volume change issue for achieving superior electrochemical performances.[3,11] Additionally, SnO_2-based anodes also suffer from limited reaction kinetics. In particular, they lack the ability to maintain excellent rate capability and ideal reversibility under high rates due to the lack of sufficient ion transport pathway, favorable electronic transfer framework, and stable electrochemical reaction interface.

Considerable effort has been made to address these problems toward tailored synthesis of SnO_2-based materials through the well-accepted nanoscale engineering, mainly including couple with conductive matrix,[12−18] fabrication of various nanostructures (such as nanowires, nano spheres, and nanoflowers),[3,19,20] as well as introduction of porous architecture.[21] Especially, the overall electrochemical performances could be further improved if any enhancement of the surface electrochemical reactivity available in SnO_2 materials.[22] It is believed to be a more suitable strategy to reduce the size and dimension of SnO_2 materials for fabricating surface-dominated ultrathin 2D structure. Just very recently, 2D nanostructures have attracted enormous attentions for great potential in lithium storage because of their exceptional structural and surface properties.[23−28] In general, their molecular-scale thickness could represent an ultrahigh surface atom percentage with great efficient active sites and specific facet exposed outside, which could convert almost electrochemical active materials into surfaces offering more lithium-insertion channels and allowing ultrafast surface lithium storage due to the shortened transport

Received: November 8, 2014
Accepted: January 16, 2015
Published: January 16, 2015

DOI: 10.1021/am507826d
ACS Appl. Mater. Interfaces 2015, 7, 2745−2753

length of lithium ions and electrons as well as the elimination of ion diffusion process in bulk.[29] Additionally, 2D nanostructures could also possess sufficient extra free space, which can alleviate the structural strain and accommodate the large volume variation to endow long-term cycling stability. Hence, the fabrication of 2D ultrathin SnO_2 nanostructure would be highly desirable for application as advanced anode materials in lithium ion batteries.

Despite an abundance of well-developed synthetic strategies toward 2D nanostructure, the observed formations are mainly limited to the layered graphene-like compounds with strong intralayer chemical bonding and weak interlayer interaction.[30−32] By contrast, nonlayered metal oxides, such as SnO_2 and TiO_2, have a strong tendency to 3D close-packed structures due to their low anisotropy. Their 2D anisotropic growth lacks larger intrinsic driving force and the relevant ultrathin structures with considerable under-coordinated surface atoms are difficult to stabilize. Although the formation of ultrathin SnO_2 nanosheets could be accomplished by previously reported surfactant-assisted solution-phase method,[6,33,34] their employed hydrothermal procedure is conducted in a sealed reactor requiring high temperature and pressure together with severe reaction parameters, making it high-cost, low yield, and time-consuming. Chen et al. reported the fabrication of phase-pure SnO_2 nanosheets with different hierarchical structures via a facile hydrothermal method.[35] It was found that the nanosheet formation is highly dependent on ammonium fluoride (NH_4F) additive with the relative amount ratio between Sn^{2+} and F^-. Their flower-like structures assembled from these nanosheets could be further tailored by adding a small amount of polyvinylpyrrolidone (PVP). Through the hydrothermal method, other nanosheet-assembled SnO_2 hollow microspheres were also synthesized by Zhao and coauthors.[36] However, their employed hydrothermal procedures are time-consuming and require high temperature, the former at 200 °C for 20 h, and the latter at 180 °C for 24 h. Accordingly, the simple, large-scale and cost-efficient synthesis of 2D ultrathin SnO_2 nanostructures has met with limited success. With respect to the potentially commercial application of the SnO_2-based anode materials, it is highly necessary to develop a simple and cost-efficient strategy to synthesize 2D ultrathin SnO_2 nanostructures at large scale.

Herein, we first present a simple and scalable synthesis of 2D ultrathin SnO_2 nanosheets through ultrarapid microwave-assisted solution-phase growth under low-temperature atmospheric conditions. As an innovative synthetic tool, microwave-assisted synthesis has been demonstrated to be an efficient and fast synthesis technique. As for the nonlayered tetragonal SnO_2, their 2D anisotropic growth in solution is achievable only if the inherent lack of larger self-driving force is compensated by additional interactions. Additionally, the crystal growth behavior could be tailored with the help of organics or polymers, such as surfactants, ligands, or capping agents.[37−39] Herein, we combine the inductive effect of microwave irradiation and structure directing of CTAB and HMT to synthesize and stabilize SnO_2 nanosheets. The rapid microwave heating can provide comfortable thermodynamic and kinetic factors to facilitate the super saturation of reactant species, leading to the instantaneous formation of ultrafine nanocrystals and then spontaneous self-assembling or oriented attachment.[31] The use of microwave irradiation makes it time-saving and high-efficiency. The whole fabrication is conducted under moderate conditions within simple reagents and equipment. The reaction system is open to air and independent of high-pressure vessels. Obviously different from the traditional method, the designed microwave synthesis does not need seeding protocols or ultrafine control over the temperature and pressure. The approach is easily scaled up to synthesize 2D ultrathin SnO_2 nanosheets in high yield, demonstrating it to be very cost-effective and greatly competitive for industrialized production. The as-synthesized SnO_2 nanosheets show a graphene-like morphology with high specific surface area and unique porous structures. X-ray photoelectron spectroscopy (XPS) measurement demonstrates an intrinsic nonstoichiometry arising from oxygen vacancies resulting into presence of Sn(II) to a certain extent. Considering the key role of surface in electrochemical reaction, we have finally examined the overall electrochemical performances of the 2D ultrathin SnO_2 nanosheets as anode for lithium ion batteries and compared the results with that of the typical 1D SnO_2 nanorods. It is found that SnO_2 nanosheets could deliver remarkablly enhanced performances over their counterparts.

2. EXPERIMENTAL SECTION

2.1. Materials Synthesis. Synthesis of SnO_2 nanosheets: The SnO_2 nanosheets were prepared through a microwave-assisted method as introduced in our previously reported work.[31] In a typical procedure, 9.6 mmol of $SnCl_2{\cdot}2H_2O$ (2.1662 g), 3.84 mmol of CTAB (Hexadecyltrimethylammonium, 1.3995 g, 16 mM), and 9.6 mmol of HMT (Hexamethylenetetramine, 1.3458 g) were initially added into 240 mL deionized water. After vigorous stirring for 30 min, the mixture was transferred into a 1000 mL homemade round-bottomed flask. A SINEO MAS-II microwave reactor (Sineo Microwave Chemistry Technology Co., LTD, Shanghai China) was employed to provide microwave irradiation under a setting mode with heating power of 700 W and heating time of 60 min. The microwave reaction procedure was monitored by a videocamera. The mixture solution was rapidly heated from room temperature to 93 °C in 2 min in an open system. After cooled down to room temperature, the postreaction system was removed out and centrifugalized. The final yellow product was obtained through wash and then dried in vacuum for about 12 h at 100 °C. To remove the possibly adsorpted organic molecular, the final product experienced a normal heat-treatment at 500 °C for 2 h.

Synthesis of SnO_2 nanorods: SnO_2 nanorods were synthesized by a traditional hydrothermal method. In a typical procedure, 0.4 g $Na_2SnO_3{\cdot}3H_2O$ and 0.28 g NaOH was initially added into 40 mL ethanol/water (1:1 v/v) mixture. After dissolved completely to form homogeneous solution, the mixture was sealed into a 50 mL Teflon-lined autoclave. The reactor was put into an oven and heated at 200 °C for 24 h. After cooled down to room temperature naturally, white precipitates were obtained. The final product was collected through centrifuging, wash and drying. For comparing the electrochemical performances, the SnO_2 nanorods were also treated at 500 °C for 2 h.

2.2. Structure Characterization. The X-ray diffraction technology was employed to detect the crystal phase of the as-prepared samples on XRD machine (Bruker D8) using Cu Kα (λ = 0.15418 nm) radiation. The morphology of the samples were investigated by electron microscopy. FESEM images were collected on Hitachi S-4800 microscope, and TEM measurements were conducted on JSM-2100F instrument with 200 kV accelerating voltage. The energy-dispersive X-ray spectroscopy was recorded coupled with TEM observation. The composition and electronic state of the SnO_2 nanosheets were determined by X-ray photoelectron sperctra (XPS, PHI Quanteral II, Japan). A NOVA4200e nitrogen adsorption instrument (Quantachrome Instruments, U.S.A.) was used to evaluate the Brunauer−Emmett−Teller specific surface areas (BET) and porosity of the samples.

2.3. Electrochemical Measurements. Electrochemical measurements were performed following the procedure reported in our

DOI: 10.1021/am507826d
ACS Appl. Mater. Interfaces 2015, 7, 2745−2753

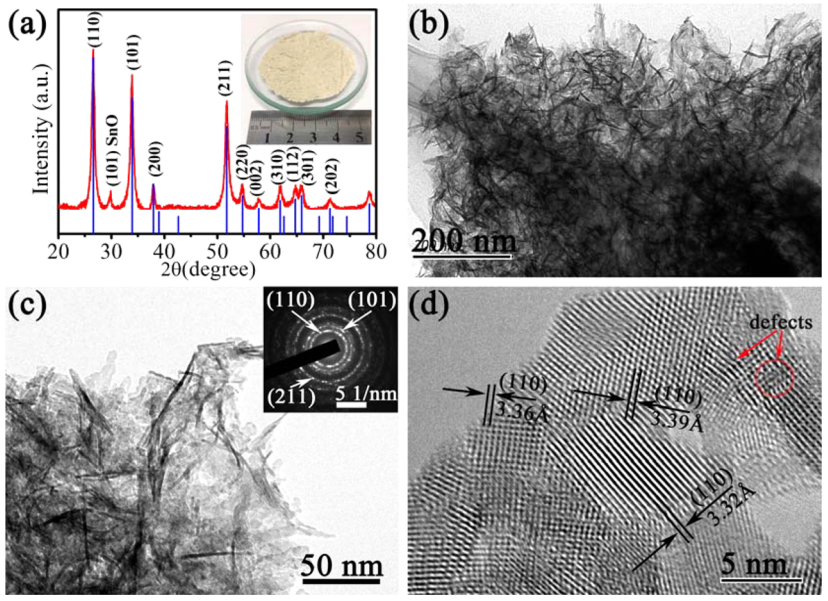

Figure 1. (a) XRD pattern, (b) and (c) TEM images, and (d) HRTEM image of the SnO_2 nanosheets, the insets in (a) and (c) show the optical photographs of SnO_2 samples through one synthetic process and the corresponding SAED pattern, respectively.

previous work.[24] Generally, a two-electrode system was constructed to collect all the electrochemical data under room temperature. High-purity metal lithium foil was used as both reference and counter electrodes. The 80 wt % prepared samples were mixed with 10 wt % Super P carbon and 10 wt % polyvinylidene fluoride (PVDF) in 1-methyl-2-pyrrolidinone (NMP) to form slurry and then cast onto the current collector (Cu foil) followed by drying at 80 °C for about 12 h in a vacuum oven. After compressed at 1.0×10^6 Pa for 30s, the Cu foil were punched into 14 mm in diameter used as working electrode. The active material loading in each disk was weighed to be 1−2 mg, corresponding to ∼1.0 mg cm^{-2}. Then CR2025-type coin cells were assembled in an Ar-filled glovebox (Universal 2440/750, Mikrouna (China) Co., Ltd.) with gas purification system monitoring the concentrations of water vapor and oxygen below 1 ppm. The electrochemical performances were measured on a CT2001A Land battery testing systems (Hannuo Electronics Co., Ltd. China) and IM6e electrochemical workstation (Zahner, Germany).

3. RESULTS AND DISCUSSION

In this work, ultrathin SnO_2 nanosheets have been successfully synthesized through a microwave-assisted wet chemistry method at large-scale. After under microwave irradiation for 60 min, the yellow product is obtained, which is in the common color resulting from the application of $SnCl_2{\cdot}2H_2O$ precursor due to the incompletion of the oxidation process. When experiencing a normal heat-treatment, the weight of the final product is measured to be ∼1.63 g per experimental run (inset in Figure1a). The crystal structure and phase purity of the as-synthesized sample were determined by XRD (Figure 1a). All the identified main diffraction peaks can be indexed to a tetragonal rutile-like SnO_2 (JCPDF card no. 41−1445; space group: $P4_2/mnm$; a_0 = 4.738 Å, c_0 = 3.1865 Å). The strong and sharp peaks suggest a high crystallinity. However, a remarkable impurity peak is found at 2θ = 29.8°, indexed to the (101) planes of SnO (JCPDF card no. 06−0395), which demonstrates a mixture phase consisted by main phase of SnO_2 and minor phase of SnO detected at XRD level. Additionally, only a very low main diffraction peak is found for SnO phase, suggesting a low content in the final sample. Figure 1b shows that the as-obtained SnO_2 sample exhibits a geometrically sheet-like 2D configuration, which manifests a similar morphology with the ever reported nanosheets.[6,33,34,40] They possess a clear and well-defined outline with large lateral size. The highly flexible and transparent features could reveal an ultrathin thickness. The magnified region selected on edge of the sheet (Figure 1c) shows that these ultrathin nanosheets spontaneously bend and fold to become weaved together leaving a porous architecture. As shown in the SAED pattern (inset in Figure 1c), the overall SnO_2 nanosheets exhibit a polycrystalline nature. The three marked diffraction rings can be indexed to the (110), (101), and (211) plane of rutile-type SnO_2. As shown in the HRTEM image (Figure 1d), the atom arrangements are clearly visible and all three local crystal planes are detected as the same (110) plane, suggesting the high degree of [001] orientation. Additionally, it is also found that amount of defects and small irregular pores are randomly distributed on the surface of the SnO_2 nanosheets, leading to a high surface roughness.

Generally, the ultrathin 2D nanomaterials are distinguished by molecular-scale thickness usually less than 5 nm. In order to determine the thickness of the SnO_2 nanosheets, further HRTEM investigation focusing on the proper edge areas was carried out. As shown in Figure 2, the transparent regions suggest planar or bended thin sheets parallel to the support substrate, whereas the dark fringe-like regions indicate some perpendicular sheets. The planar region also exhibits clear and regular lattice fringes with a lattice spacing of 0.339 nm, which is corresponding to (110) planes. The widths of the marked dark regions are measured to be 1.9, 2.4, and 2.8 nm, suggesting the SnO_2 nanosheets with a thickness of 2−3 nm.

It is well-known that the bottom-up growth of most nanomaterials is significantly affected by different reaction conditions leading to various microstructures and morphologies. In our designed solution-phase system, we choose HMT as the alkaline reagents and CTAB as surfactant. The tetragonal rutile-like SnO_2 belongs to $P42/mnm$ space group with lattice constant $a_0 = b_0$ = 4.738 Å, c_0 = 3.1865 Å. The low crystallographic anisotropy brings it a strong tendency to 3D close-packed microstructures and morphologies. Their 2D

DOI: 10.1021/am507826d
ACS Appl. Mater. Interfaces 2015, 7, 2745−2753

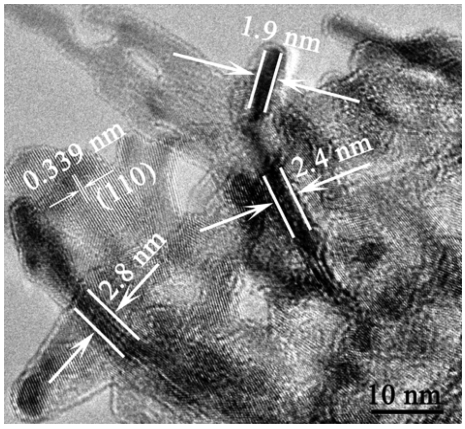

Figure 2. HRTEM image of the SnO_2 nanosheets showing the thickness to be 2−3 nm.

anisotropic growth is hard to achieve for the lack of larger intrinsic driving force. It has been reported that surfactant could regulate the crystal growth behavior. In order to investigate the effect of surfactant on the morphology of synthesized SnO_2, we carried out the synthesis at various amount of CTAB. Figure 3

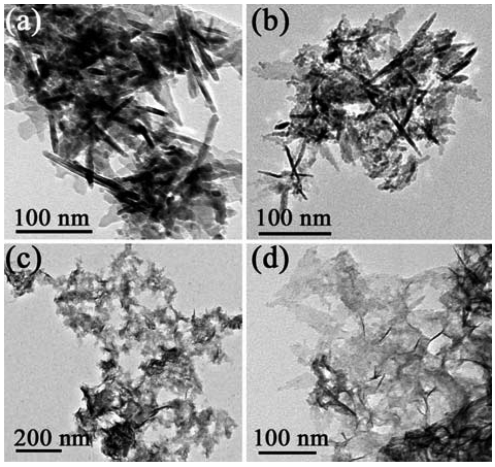

Figure 3. TEM images of the SnO_2 samples synthesized at various amount of CTAB, (a) 0 mM, (b) 8 mM, and (c) and (d) 32 mM.

shows the TEM images of the SnO_2 samples. It can be clearly found that the added CTAB plays an important role in the morphology formation of the final products. When without assistance of CTAB (Figure 3a), the uniform 2D nanosheets could hardly form; instead, most of the products exhibit ultrathin irregular rod-like structure. After adding a small amount of CTAB (8 mM), the rod-like structure turns out relatively rare leaving more ultrafine nanosheets (Figure 3b). We then further increased the amount of CTAB up to 32 mM, two times as that used for electrochemical measurement. As shown in Figure 3c and d, the products also preserve sheet-like morphology similar to that synthesized at 16 mM concentration of CTAB but with high dispersivity. So the added CTAB is key parameter in controlling microstructures and morphologies of the final SnO_2 samples.

Energy dispersive X-ray spectroscopy (EDS) analysis was first employed to confirm the elementary composition of the synthesized SnO_2 samples. As shown in Figure 4a, besides the C signal coming from the substrate, only Sn and O are

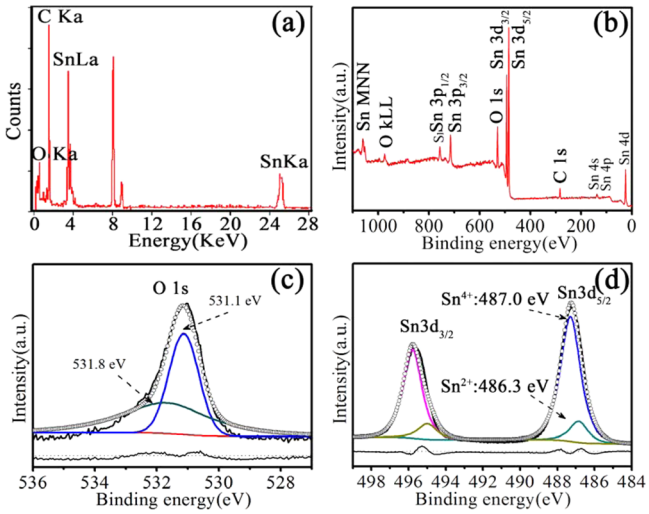

Figure 4. (a) EDS pattern, (b) XPS full spectrum, (c) the deconvoluted O 1s, and (d) Sn 3d spectra of the SnO_2 nanosheets.

detected. The composition and surface electronic state of the SnO_2 nanosheets were carefully investigated by XPS analysis. In the full spectrum (Figure 4b), only Sn, O, and C elements are detected. The binding energy of C 1s peak at 284.6 eV is used as the reference point for charge correcting. No other peaks are observed, thus indicating high purity of the samples. The O 1s emission spectrum could be divided into two main peaks (Figure 4c). The peak at 531.1 eV is typical of metal−oxygen bonds, whereas the peak at 531.8 eV is associated with oxygen ions in low coordination at the surface leading to non-stoichiometric defects in SnO_2 nanosheets. The deconvoluted core level spectra of the Sn 3d region are shown in Figure 4d. The observed two strong peaks are ascribed to Sn $3d_{5/2}$ and Sn $3d_{3/2}$, indicating the Sn^{4+} oxidation state. However, both of them fall into an asymmetrical shape, which suggest that each Sn 3d peak could be respectively deconvoluted into two peaks. The deconvoluted minor peaks are ascribed to Sn^{2+} in the matrix. The chemical shift between Sn^{4+} and Sn^{2+} is ∼0.7 eV, close to that previously reported.[33] Some Sn^{4+} ions are reduced to Sn^{2+} state through charge compensation due to the nonstoichiometric oxygen deficiency caused by oxygen vacancies.[41] It is believable that the considerable surface defects and oxygen vacancies can help balance their excessive surface energy and then maintain an excellent structural stability.[42]

Nitrogen adsorption−desorption isothermal measurement was further carried out to investigate the surface-dominated 2D structure of SnO_2 nanosheets. Figure 5 shows the Nitrogen adsorption−desorption isotherms and the corresponding pore size distribution (inset) of SnO_2 nanosheets. The isotherm belongs to a type IV with a type H3 hysteresis loop, indicating a typical mesoporous structure. The SnO_2 nanosheets exhibit a BET specific surface area of 135.7 $m^2\ g^{-1}$ with a total pore volume of 0.7911 $cm^3\ g^{-1}$. Such a high value could arise from the unique structure of the ultrathin 2D nanosheets with rough surfaces. The most probable pore size is 2.18 nm using the Barrett−Joyner−Halenda model. The pores in a wide size range should stem from the restack of the sheets. The large surface area of the ultrathin 2D nanosheets may significantly reduce the Li-ion diffusion length, providing more electrochemical active sites and ultrafast surface lithium storage, which could result in enhanced electrochemical lithium storage properties.

DOI: 10.1021/am507826d
ACS Appl. Mater. Interfaces 2015, 7, 2745−2753

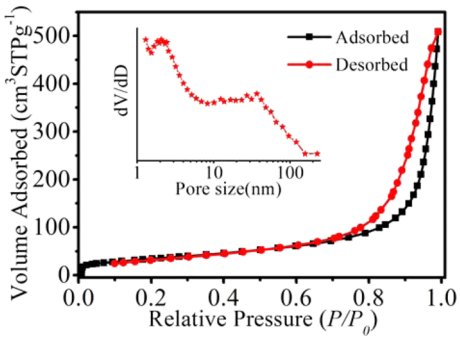

Figure 5. N_2 adsorption−desorption isotherm of the SnO_2 nanosheets, the inset showing the pore size distributions.

2D nanostructures are of great interest for lithium storage owing to their unique structural properties and surface characteristics.[3,23,29] The electrochemical reactivity of the as-synthesized SnO_2 nanosheets is first examined through cyclic voltammograms (CVs) at a scan rate of 0.1 mVs^{-1} in the potential window of 0−2.0 V vs Li/Li^+. Figure 6a shows the first five representative CV curves of lithiation/delithiation processes to reveal the electrochemical lithium storage mechanism, and the CV behavior is generally consistent with previous reports.[43] In the first scan, two obvious peaks appear in the cathodic process, located around 0.76 and 0.12 V, respectively. The sharp and well-defined irreversible reduction peak at 0.76 V is ascribed to initial reduction of SnO_2 to Sn, the synchronous formation of Li_2O and solid electrolyte interphase (SEI) layer.[44] The reduction peak at 0.12 V corresponds to the formation of a series of Li_xSn alloys. In the anodic process, the oxidation peak around 0.56 V stands for dealloying of the Li_xSn. During the subsequent cycles, both of the two reversible peaks relevant to alloying/dealloying divide into three individual peak, including three reduction peaks (at 0.57, 0.28, and 0.10 V) and three oxidation peaks (at 0.77, 0.63, and 0.51 V). The visible division reveals that the active materials uptake different electrochemical reactions in the subsequent cycles, which are much closer to stoichiometric reaction. The position of the main oxidation peak shifts to the lower potential direction, approaching the potential of corresponding reduction peak, which could indicate the higher reversibility. It is interesting to have found that a broad cathodic peak (0.9−1.3 V) and a corresponding anodic peak (1.1−1.5 V) still exist during the fifth cycle, suggesting partial reversibility of reaction related to Li_2O converting to Li^+.[33,35] After the first cycle, the CV curves become stable and overlap, indicating an excellent reversibility of the electrochemical reaction and good cycling stability as discussed below.

It is an efficient strategy to employ various 1D SnO_2-based materials such as nanorods and nanowires for improving the lithium storage performances.[45−48] The 1D SnO_2 nanostructures could provide good electrical conductivity thus improving their electrochemical properties. Herein, we also synthesize SnO_2 nanorods (Supporting Information, SI, Figure S1 and Figure S2) for comparison. Figure 6b,c presents the discharge−charge voltage profiles for the first five cycles of SnO_2 nanosheets and SnO_2 nanorods checked at 200 mA g^{-1} current density. In the first discharge curves, they both exhibit an extended voltage plateau at ~0.95 V, followed by a sloping curve down to the cutoff voltage of 0.01 V, suggesting that the two electrodes share the same electrochemical reaction process. The first discharge and charge capacities of the SnO_2 nanosheet electrodes are 2260.7 and 1155.5 mAh g^{-1}, respectively, which are much larger than that of nanorod electrodes (1716.1 and 725.9 mAh g^{-1}). Even at a higher current density of 300 mA g^{-1} (SI Figure S3a), the SnO_2 nanosheet electrodes also could delivery high initial discharge and charge capacities of 1708.2 and 865.2 mAh g^{-1}, which are nearly equivalent to that of nanorod electrodes (1722.3 and 845.4 mAh g^{-1}) measured at 100 mA g^{-1} current density (SI Figure S3b). Generally speaking, ultrathin 2D nanomaterials could give rise to high efficient active sites exposed outside for electrochemical reaction and more lithium-insertion channels with possibile space lithium storage. As a result, ultrahigh initial discharge capacity is achieved in this kind of 2D materials. In our previous

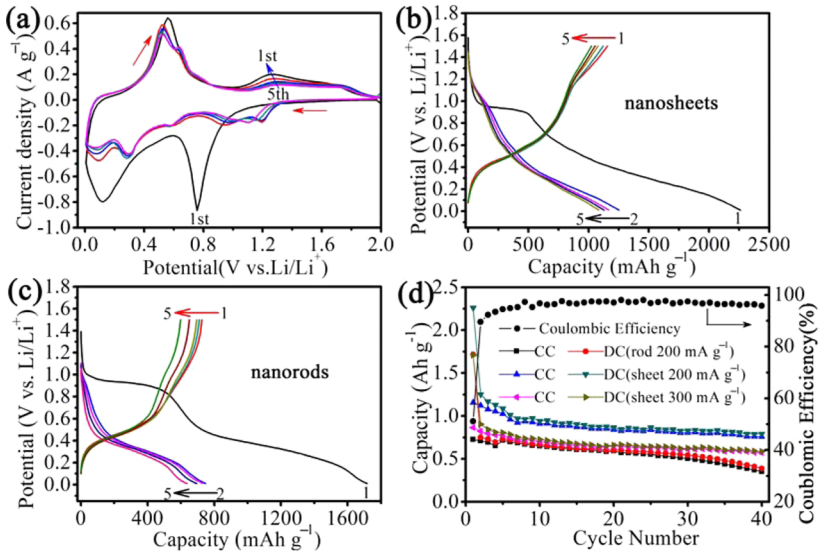

Figure 6. (a) Typical CV curves of the SnO_2 nanosheets; the first five galvanostatic charge−discharge profiles of (b) the SnO_2 nanosheets and (c) the SnO_2 nanorods at a constant current density of 200 mA g^{-1} between 0.01 and 1.5 V. (d) The charge capacity(CC) and discharge capacity(DC) as a function of cycle number of the SnO_2 nanosheets and the SnO_2 nanorods for comparison together with the Coulombic efficiency of the SnO_2 nanosheets at 200 mA g^{-1}.

DOI: 10.1021/am507826d
ACS Appl. Mater. Interfaces 2015, 7, 2745−2753

work, we prepared SnO_2/graphene hybrid as anode materials for lithium ion battery.[40] The initial discharge capacity of SnO_2/graphene hybrid is as high as 2445.7 mAh g^{-1}. We attributed the high value to the strongly coupled mesoporous structure of SnO_2/graphene hybrid. As far as we know, the initial discharge capacity of 2260.7 mAh g^{-1} delivered by our ultrathin SnO_2 nanosheets is much higher than that of other similar SnO_2 nanosheets prepared by different approaches.[6] Wang and coauthors reported a relative high initial discharge capacity of 1742 mAh g^{-1} for ultrathin SnO_2 nanosheets synthesized by hydrothermal processes,[33] but still lower than our result. In view of the surface electrochemical reaction for lithium storage in the unique ultrathin SnO_2 nanosheets, various factors, such as high specific surface area, sufficient lithium-insertion channels, favorable reaction kinetic and so on, may affect the first discharge process mainly coupled with additional capacities just demonstrated by the above-mentioned anode materials. Herein, we attribute the obvious enhancement of the initial discharge capacity for our ultrathin SnO_2 nanosheets to the high crystallinity and the complete remove of the possibile surface-absorbed organic molecular through a normal heat-treatment, which could provide more favorable surface environment for lithium ion insertion. The initial irreversible capacity losses are mainly caused by the irreversible SEI film formation.[47,49] Except the first discharge process, the SnO_2 nanosheets show a similar and early overlapped discharge−charge curve, which suggests an excellent cycling stability consistent as discussed below. By contrast, the SnO_2 nanorods exhibit an obviously separated curve, suggesting progressively severe capacity decay. As a result, the SnO_2 nanosheet electrodes deliver higher initial Coulombic efficiency of 51.1% (200 mA g^{-1}) and 50.6% (300 mA g^{-1}), close to the theoretical value (52%) and much higher that of SnO_2 nanorod electrodes of 42.3% (200 mA g^{-1}) and 49.1% (100 mA g^{-1}). The high initial Coulombic efficiency could indicate excellent electrochemical reversibility for SnO_2 nanosheets and the presence of a small amount of SnO. So it can be concluded that the unique ultrathin nanostructure can give rise to great electrochemical activities and more flexible electrode/electrolyte interfaces, which could guarantee highly reversible interfacial reaction during the lithium insertion and extraction.

Figure 6d shows the cycling performances of the SnO_2 nanosheets and the SnO_2 nanorods for comparison. The SnO_2 nanosheets exhibit excellent cycling stability at both current densities (200 and 300 mA g^{-1}), whereas the SnO_2 nanorods show serious capacity decay after the 30th cycle even if at 200 mA g^{-1} current density. When prolonged to the second discharge−charge cycle, the Coulombic efficiency of SnO_2 nanosheets (at 200 mA g^{-1}) increases to 90% and maintains at relatively high level over 95% in the subsequent cycles. The reversible capacities of the SnO_2 nanosheets could be maintained at 757.6 (at 200 mA g^{-1}) and 571.5 mAh g^{-1} (at 300 mA g^{-1}) up to the 40th cycle. The corresponding reversible capacity retention is calculated to be 65.6% and 66.1% based on the first values, respectively. Our statistical analysis further shows that the experimental results are very likely of good recurrence (see SI Figure S4, Statistical analysis of the charge capacities of the SnO_2 nanosheets at a constant current density of 200 mA g^{-1} based on four typical batteries). The calculated average initial and 40th reversible capacities of the SnO_2 nanosheets are 1125.5 and 731.2 mAh g^{-1} at 200 mA g^{-1}, which are nearly equivalent to that observed corresponding charge capacities (1155.5 and 757.6 mAh g^{-1}), respectively. On the contrary, the SnO_2 nanorods only hold a low reversible capacity of 350.9 mAh g^{-1} with retention of 48.3% at the 40th cycle. Then compared with the 1D nanorods, the 2D SnO_2 nanosheets not only delivery high initial lithium storage capacity, but also excellent cycling stability even at high current density. These results indicate that the structural feature of the 2D SnO_2 nanosheets with porous structures could provide good reaction kinetic and extra free space. As a result, the structural strain caused by the drastic volume variation during repeated Li^+ insertion/extraction processes could be well alleviated. Consequently, the excellent cycling stability is achieved in the unique 2D SnO_2 nanosheets.

Along with the excellent cycling stability, the SnO_2 nanosheets also exhibit perfect rate capability. As shown in Figure 7, the initial reversible capacity is 1164.4 mAh g^{-1} at 0.1

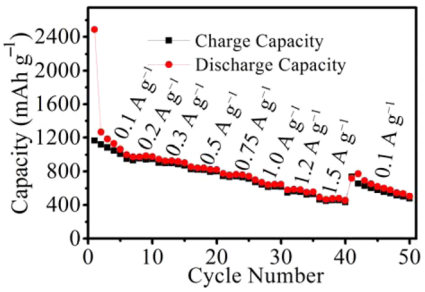

Figure 7. Rate capability of the SnO_2 nanosheets at various current densities.

A g^{-1} current density. After 5 cycles, the reversible capacity is still be maintained at 1010.1 mAh g^{-1} with high Coulombic efficiency of 94.8%. As the current densities increase from 0.2 to 0.3, 0.5, 0.75, 1.0, 1.2, and 1.5 A g^{-1}, the SnO_2 nanosheets also exhibit remarkable capacity retention, varying from 950.9, 903.9, 825.6, 743.5, 670.6, 546.9, and 464.0 mAh g^{-1}. After the highest current cycles (1.5 A g^{-1}), the reversible capacity is still be maintained at 434.0 mAh g^{-1}. When the current density is reversed back to 0.1 A g^{-1}, the reversible capacity can recover a high value of 736.0 mAh g^{-1}, which is approximately equivalent to the result (757.6 mAh g^{-1}) measured at a 200 mA g^{-1} in the corresponding cycles as shown in Figure 6d. The observed reversible capacities of SnO_2 nanosheets are well consistent with the statistical analysis results (see the SI Figure S5, Statistical analysis of rate capability of the SnO_2 nanosheets based on three typical batteries). This rate capability test indicates that the 2D SnO_2 nanostructure could deliver excellent cycling stability even under severe loading/deloading rates, which also could be contributed to the good integrity of the SnO_2 nanosheet electrode. However, it is difficult for the SnO_2 nanorods to achieve such a good rate capability. As shown in SI Figure S3c, the SnO_2 nanorods display serious capacity decay even under the relatively moderate charge/discharge manner. The excellent rate performance of the SnO_2 nanosheets could be attributed to the fact that the 2D structure could provide favorable charge-transport pathway and shorten ion diffusion length in the thickness direction. Additionally, the high specific surface area also provides large electrode−electrolyte contact area with better lithium ions access for efficient electrochemical reaction. More importantly, with respect to the ultrathin 2D architecture, almost active species are arranged into surfaces, which make it possible for ultrafast surface lithium storage.

DOI: 10.1021/am507826d
ACS Appl. Mater. Interfaces 2015, 7, 2745−2753

The favorable reaction kinetic of the SnO_2 nanosheets was further demonstrated by the electrochemical impedance spectra (EIS). Figure 8 and SI Figure S3d show the Nyquist plots of the

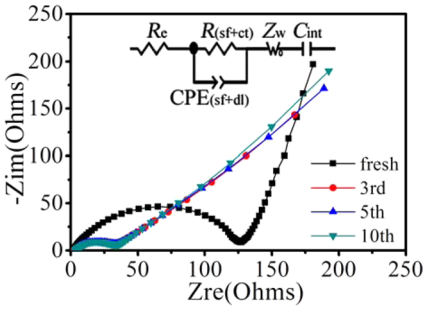

Figure 8. Nyquist plots of the SnO_2 nanosheets spectra measured at open circuit potential of ~1.2 V and the equivalent electrical circuit (inset) used to fit the experimental impedance.

as-synthesized SnO_2 nanosheets and the SnO_2 nanorods for comparison, which consist of a high frequency depressed semicircle and an inclined line in low frequency region. To interpret the Nyquist plots, we set up a possible equivalent circuit as shown in the inset of Figure 8. The contained elements represent surface film resistance (R_{sf}), ohmic resistance of the electrolyte and cell components (R_e), a constant phase element (CPE_i) (sf, double layer (dl)), charge-transfer resistance at the interface between the electrode and electrolyte (R_{ct}), Warburg impedance (Z_w), and intercalation capacitance (C_{int}).[24,50] The observed high frequency depressed semicircle is corresponding to the surface film and charge-transfer resistance $R_{(sf+ct)}$. Obviously, the fresh SnO_2 nanosheet electrodes exhibit a lower $R_{(sf+ct)}$ (124 Ω) than that of the SnO_2 nanorods (191 Ω), suggesting a more stable surface film and faster charge-transfer process for the nanosheets. Encouragingly, the SnO_2 nanosheet electrodes show much lower $R_{(sf+ct)}$ during the subsequent plots, all falling to ~30 Ω, due to much more in-depth electrochemical activation of the electrode. However, the $R_{(sf+ct)}$ of the SnO_2 nanorods is still be maintained at a range of 130−170 Ω. The markedly decreased resistance indicates the enhanced ion conductivity in the SnO_2 nanosheets, which is more beneficial for Li^+ insertion/extraction.[51] So the electron transfer and ion diffusion of the unique SnO_2 nanosheets are much faster than that of SnO_2 nanorods and thus lead to outstanding improvement on the rate performance. Additionally, the low-frequency slope angle of the SnO_2 nanosheets becomes almost the same obviously different with these varied ones of the SnO_2 nanorods, which suggests a more stable surface reactivity toward the electrolyte for nanosheets.[11] The nearly constant low $R_{(sf+ct)}$ and the same low-frequency slope angle could reveal that an ideal interfacial layer between the Sn metal and the electrolyte could be constructed during the repeated Li^+ insertion/extraction processes, which is therefore key in improving the cycling performance of the SnO_2 nanosheet electrodes. The stable interface with high flexibility is believed to accommodate the volumetric expansion of SnO_2-based anode without mechanical damage.

4. CONCLUSIONS

In summary, we have successfully synthesized the 2D ultrathin SnO_2 nanosheets by microwave-assisted solution-phase growth for the first time. The innovative method has been demonstrated to be ultrarapid, simple, and time-saving. What is far more important is that the microwave-assisted method is easily scaled up, which makes it rather cost-effective and greatly competitive for industrialized production. The weight of the final ultrathin 2D SnO_2 nanosheets is ~1.63 g by one time in the present synthetic system. The 2D anisotropic growth SnO_2 nanosheets depends on the microwave dielectric irradiating coupled with surfactant structural directing. Electrochemical measurements show that the ultrathin SnO_2 nanosheets exhibit remarkably improved electrochemical lithium storage properties with a high reversible capacity of 757.6 mAh g^{-1} at 200 mA g^{-1} in 40 cycles as well as excellent cycling stability and rate capability in comparison with 1D SnO_2 nanorods. The enhanced lithium storage properties could be contributed to the efficient surface electrochemical reaction facilitated by the high-quality ultrathin 2D nanostructure, which could guarantee more lithium-storage sites, shorter lithium-ion diffusion length, fast electron transfer, and sufficient void space to buffer the volume variation.

■ ASSOCIATED CONTENT

Supporting Information

Galvanostatic charge−discharge curves of the SnO_2 nanosheets (300 mA g^{-1}); XRD pattern, FESEM image, galvanostatic charge−discharge curves (100 mA g^{-1}), rate capability, Nyquist plots of the SnO_2 nanorods, and Statistical analysis of the charge capacities and rate capability of the SnO_2 nanosheets. This material is available free of charge via the Internet at http://pubs.acs.org.

■ AUTHOR INFORMATION

Corresponding Authors

*Tel: +86 10 68913792; fax: +86 10 68912001; e-mail: huazhzhai@bit.edu.cn.

*Tel: +86 10 68913792; fax: +86 10 68912001; e-mail: cbcao@bit.edu.cn.

Author Contributions

The manuscript was written through contributions of all authors. All authors have given approval to the final version of the manuscript.

Notes

The authors declare no competing financial interest.

■ ACKNOWLEDGMENTS

This work was financially supported by the National Natural Science Foundation of China (Grant Nos. 51272029 and 21371023) and Research Fund for the Doctoral Program of Higher Education of China (Grant No. 20101101110026).

■ REFERENCES

(1) Chen, Z.; Zhou, M.; Cao, Y.; Ai, X.; Yang, H.; Liu, J. In-Situ Generation of Few-Layer Graphene Coatings on SnO_2−SiC Core-Shell Nanoparticles for High-Performance Lithium-Ion Storage. *Adv. Energy Mater.* **2012**, *2*, 95−102.

(2) Lou, X. W.; Li, C. M.; Archer, L. A. Designed Synthesis of Coaxial SnO_2@Carbon Hollow Nanospheres for Highly Reversible Lithium Storage. *Adv. Mater.* **2009**, *21*, 2536−2539.

(3) Deng, J.; Yan, C.; Yang, L.; Baunack, S.; Oswald, S.; Wendrock, H.; Mei, Y.; Schmidt, O. G. Sandwich-Stacked SnO_2/Cu Hybrid Nanosheets as Multichannel Anodes for Lithium Ion Batteries. *ACS Nano* **2013**, *7*, 6948−6954.

(4) Ebner, M.; Marone, F.; Stampanoni, M.; Wood, V. Visualization and Quantification of Electrochemical and Mechanical Degradation in Li Ion Batteries. *Science* **2013**, *342*, 716−720.

DOI: 10.1021/am507826d
ACS Appl. Mater. Interfaces 2015, 7, 2745−2753

(5) Li, X.; Meng, X.; Liu, J.; Geng, D.; Zhang, Y.; Banis, M. N.; Li, Y.; Yang, J.; Li, R.; Sun, X.; Cai, M.; Verbrugge, M. W. Tin Oxide with Controlled Morphology and Crystallinity by Atomic Layer Deposition onto Graphene Nanosheets for Enhanced Lithium Storage. *Adv. Funct. Mater.* **2012**, *22*, 1647−1654.
(6) Wang, C.; Zhou, Y.; Ge, M.; Xu, X.; Zhang, Z.; Jiang, J. Z. Large-Scale Synthesis of SnO_2 Nanosheets with High Lithium Storage Capacity. *J. Am. Chem. Soc.* **2010**, *132*, 46−47.
(7) Tarascon, J. M.; Armand, M. Issues and Challenges Facing Rechargeable Lithium Batteries. *Nature* **2001**, *414*, 359−367.
(8) Noh, M.; Kim, Y.; Kim, M. G.; Lee, H.; Kim, H.; Kwon, Y.; Lee, Y.; Cho, J. Monomer-Capped Tin Metal Nanoparticles for Anode Materials in Lithium Secondary Batteries. *Chem. Mater.* **2005**, *17*, 3320−3324.
(9) Wang, H.; Rogach, A. L. Hierarchical SnO_2 Nanostructures: Recent Advances in Design, Synthesis, and Applications. *Chem. Mater.* **2014**, *26*, 123−133.
(10) Ding, S.; Luan, D.; Boey, F. Y. C.; Chen, J. S.; Lou, X. W. SnO_2 Nanosheets Grown on Graphene Sheets with Enhanced Lithium Storage Properties. *Chem. Commun.* **2011**, *47*, 7155−7157.
(11) Zheng, G.; Lee, S. W.; Liang, Z.; Lee, H. W.; Yan, K.; Yao, H.; Wang, H.; Li, W.; Chu, S.; Cui, Y. Connected Hollow Carbon Nanospheres for Stable Lithium Metal Anodes. *Nat. Nanotechnol.* **2014**, *9*, 618−623.
(12) Paek, S. M.; Yoo, E.; Honma, I. Enhanced Cyclic Performance and Lithium Storage Capacity of SnO_2/Graphene Nanoporous Electrodes with Three-Dimensionally Delaminated Flexible Structure. *Nano Lett.* **2009**, *9*, 72−75.
(13) Wang, L.; Wang, D.; Dong, Z.; Zhang, F.; Jin, J. Interface Chemistry Engineering for Stable Cycling of Reduced GO/SnO_2 Nanocomposites for Lithium Ion Battery. *Nano Lett.* **2013**, *13*, 1711−1716.
(14) Chen, G.; Wang, Z.; Xia, D. One-Pot Synthesis of Carbon Nanotube@SnO_2-Au Coaxial Nanocable for Lithium-Ion Batteries with High Rate Capability. *Chem. Mater.* **2008**, *20*, 6951−6956.
(15) Zhang, C.; Peng, X.; Guo, Z. P.; Cai, C.; Chen, Z.; Wexler, D.; Li, S.; Liu, H. K. Carbon-Coated SnO_2/Graphene Nanosheets as Highly Reversible Anode Materials for Lithium Ion Batteries. *Carbon* **2012**, *50*, 1897−1903.
(16) Zhang, C.; Quince, M.; Chen, Z.; Guo, Z. P.; Liu, H. K. Three-Dimensional Nanocarbon and the Electrochemistry of Nanocarbon/Tin Oxide for Lithium Ion Batteries. *J. Solid State Electrochem.* **2011**, *15*, 2645−2652.
(17) Wen, Z.; Wang, Q.; Zhang, Q.; Li, J. In Situ Growth of Mesoporous SnO_2 on the Multiwalled Carbon Nanotubes: A Novel Composite with Porous-Tube Structure as Anode for Lithium Batteries. *Adv. Funct. Mater.* **2007**, *17*, 2772−2778.
(18) Li, Y.; Lv, X.; Lu, J.; Li, J. Preparation of SnO_2−Nanocrystal/Graphene-Nanosheets Composites and Their Lithium Storage Ability. *J. Phys. Chem. C* **2010**, *114*, 21770−21774.
(19) Bhaskar, A.; Deepa, M.; Rao, T. N. Size-Controlled SnO_2 Hollow Spheres via a Template Free Approach as Anodes for Lithium Ion Batteries. *Nanoscale* **2014**, *6*, 10762−10771.
(20) Hassan, M. F.; Rahman, M. M.; Guo, Z. P.; Chen, Z.; Liu, H. K. SnO_2−NiO−C Nanocomposite as a High Capacity Anode Material for Lithium-Ion Batteries. *J. Mater. Chem.* **2010**, *20*, 9707−9712.
(21) Yang, T.; Lu, B. Highly Porous Structure Strategy to Improve the SnO_2 Electrode Performance for Lithium-Ion Batteries. *Phys. Chem. Chem. Phys.* **2014**, *16*, 4115−4121.
(22) Poizot, P.; Laruelle, S.; Grugeon, S.; Dupont, L.; Tarascon, J. M. Nano-Sized Transition-Metal Oxides as Negative-Electrode Materials for Lithium-Ion Batteries. *Nature* **2000**, *407*, 496−499.
(23) Yoo, E.; Kim, J.; Hosono, E.; Zhou, H.; Kudo, T.; Honma, I. Large Reversible Li Storage of Graphene Nanosheet Families for Use in Rechargeable Lithium Ion Batteries. *Nano Lett.* **2008**, *8*, 2277−2282.
(24) Zhu, Y.; Guo, H.; Wu, Y.; Cao, C.; Tao, S.; Wu, Z. Surface-Enabled Superior Lithium Storage of High-Quality Ultrathin NiO Nanosheets. *J. Mater. Chem. A* **2014**, *2*, 7904−7911.
(25) Rangappa, D.; Murukanahally, K. D.; Tomai, T.; Unemoto, A.; Honma, I. Ultrathin Nanosheets of Li_2MSiO_4 (M = Fe, Mn) as High-Capacity Li-Ion Battery Electrode. *Nano Lett.* **2012**, *12*, 1146−1151.
(26) Zhu, J.; Li, Q.; Bi, W.; Bai, L.; Zhang, X.; Zhou, J.; Xie, Y. Ultra-Rapid Microwave-Assisted Synthesis of Layered Ultrathin Birnessite $K_{0.17}MnO_2$ Nanosheets for Efficient Energy Storage. *J. Mater. Chem. A* **2013**, *1*, 8154−8159.
(27) Du, Y.; Yin, Z.; Zhu, J.; Huang, X.; Wu, X. J.; Zeng, Z.; Yan, Q.; Zhang, H. A General Method for the Large-Scale Synthesis of Uniform Ultrathin Metal Sulphide Nanocrystals. *Nat. Commun.* **2012**, *3*, 1177.
(28) Wang, H.; Feng, H.; Li, J. Graphene and Graphene-like Layered Transition Metal Dichalcogenides in Energy Conversion and Storage. *Small* **2014**, *11*, 2165−2181.
(29) Liu, J.; Liu, X. W. Two-Dimensional Nanoarchitectures for Lithium Storage. *Adv. Mater.* **2012**, *24*, 4097−4111.
(30) Duan, H.; Yan, N.; Yu, R.; Chang, C. R.; Zhou, G.; Hu, H. S.; Rong, H.; Niu, Z.; Mao, J.; Asakura, H.; Tanaka, T.; Dyson, P. J.; Li, J.; Li, Y. Ultrathin Rhodium Nanosheets. *Nat. Commun.* **2014**, *5*, 3093.
(31) Zhu, Y.; Cao, C.; Tao, S.; Chu, W.; Wu, Z.; Li, Y. Ultrathin Nickel Hydroxide and Oxide Nanosheets: Synthesis, Characterizations and Excellent Supercapacitor Performances. *Sci. Rep.* **2014**, *4*, 5787.
(32) Radisavljevic, B.; Radenovic, A.; Brivio, J.; Giacometti, V.; Kis, A. Single-Layer MoS_2 Transistors. *Nat. Nanotechnol.* **2011**, *6*, 147−150.
(33) Wang, C.; Du, G.; Ståhl, K.; Huang, H.; Zhong, Y.; Jiang, J. Z. Ultrathin SnO_2 Nanosheets: Oriented Attachment Mechanism, Nonstoichiometric Defects, and Enhanced Lithium-Ion Battery Performances. *J. Phys. Chem. C* **2012**, *116*, 4000−4011.
(34) Sun, Y.; Lei, F.; Gao, S.; Pan, B.; Zhou, J.; Xie, Y. Atomically Thin Tin Dioxide Sheets for Efficient Catalytic Oxidation of Carbon Monoxide. *Angew. Chem., Int. Ed.* **2013**, *52*, 10569−10572.
(35) Chen, J. S.; Ng, M. F.; Wu, H. B.; Zhang, L.; Lou, X. W. Synthesis of Phase-Pure SnO_2 Nanosheets with Different Organized Structures and Their Lithium Storage Properties. *CrystEngComm* **2012**, *14*, 5133−5136.
(36) Zhao, X.; Cao, M.; Hu, C. Binder Strategy towards Improving the Rate Performance of Nanosheet-Assembled SnO_2 Hollow Microspheres. *RSC Adv.* **2012**, *2*, 11737−11742.
(37) Niu, Z.; Li, Y. Removal and Utilization of Capping Agents in Nanocatalysis. *Chem. Mater.* **2014**, *26*, 72−83.
(38) Tang, Z.; Zhang, Z.; Wang, Y.; Glotzer, S. C.; Kotov, N. A. Self-Assembly of CdTe Nanocrystals into Free-Floating Sheets. *Science* **2006**, *314*, 274−278.
(39) Yu, T.; Lim, B.; Xia, Y. Aqueous-Phase Synthesis of Single-Crystal Ceria Nanosheets. *Angew. Chem., Int. Ed.* **2010**, *49*, 4484−4487.
(40) Zhu, Y.; Li, C.; Cao, C. Strongly Coupled Mesoporous SnO_2−Graphene Hybrid with Enhanced Electrochemical and Photocatalytic Activity. *RSC Adv.* **2013**, *3*, 11860−11868.
(41) Godinho, K. G.; Walsh, A.; Watson, G. W. Energetic and Electronic Structure Analysis of Intrinsic Defects in SnO_2. *J. Phys. Chem. C* **2009**, *113*, 439−448.
(42) Sun, Y.; Sun, Z.; Gao, S.; Cheng, H.; Liu, Q.; Piao, J.; Yao, Tao.; Wu, C.; Hu, S.; Wei, S.; Xie, Y. Fabrication of Flexible and Freestanding Zinc Chalcogenide Single Layers. *Nat. Commun.* **2012**, *3*, 1057.
(43) Wu, S.; Wang, M.; Li, C.; Zhu, Y.; Wang, H. Single Crystalline SnO_2 Nanowires Obtained from Heat-Treated SnO_2 and C Mixture and Their Electrochemical Properties. *Mater. Chem. Phys.* **2014**, *147*, 184−190.
(44) Wang, D.; Li, X.; Wang, J.; Yang, J.; Geng, D.; Li, R.; Cai, M.; Sham, T. K.; Sun, X. Defect-Rich Crystalline SnO_2 Immobilized on Graphene Nanosheets with Enhanced Cycle Performance for Li Ion Batteries. *J. Phys. Chem. C* **2012**, *116*, 22149−22156.
(45) Kim, H.; Cho, J. Hard Templating Synthesis of Mesoporous and Nanowire SnO_2 Lithium Battery Anode Materials. *J. Mater. Chem.* **2008**, *18*, 771−775.
(46) Ren, W.; Wang, C.; Lu, L.; Li, D.; Cheng, C.; Liu, J. SnO_2@Si Core-Shell Nanowire Arrays on Carbon Cloth as a Flexible Anode for Li Ion Batteries. *J. Mater. Chem. A* **2013**, *1*, 13433−13438.

DOI: 10.1021/am507826d
ACS Appl. Mater. Interfaces 2015, 7, 2745−2753

(47) Wu, P.; Du, N.; Zhang, H.; Yu, J.; Qi, Y.; Yang, D. Carbon-Coated SnO_2 Nanotubes: Template-Engaged Synthesis and Their Application in Lithium-Ion Batteries. *Nanoscale* **2011**, *3*, 746−750.
(48) Tang, Y.; Wu, D.; Chen, S.; Zhang, F.; Jia, J.; Feng, X. Highly Reversible and Ultra-Fast Lithium Storage in Mesoporous Graphene-Based TiO_2/SnO_2 Hybrid Nanosheets. *Energy Environ. Sci.* **2013**, *6*, 2447−2451.
(49) Kravchyk, K.; Protesescu, L.; Bodnarchuk, M. I.; Krumeich, F.; Yarema, M.; Walter, M.; Guntlin, C.; Kovalenko, M. V. Monodisperse and Inorganically Capped Sn and Sn/SnO_2 Nanocrystals for High-Performance Li-Ion Battery Anodes. *J. Am. Chem. Soc.* **2013**, *135*, 4199−4202.
(50) Zhou, G.; Wang, D. W.; Yin, L. C.; Li, N.; Li, F.; Cheng, H. M. Oxygen Bridges between NiO Nanosheets and Graphene for Improvement of Lithium Storage. *ACS Nano* **2012**, *6*, 3214−3223.
(51) Li, P.; Zhao, G.; Cui, X.; Zhang, Y.; Tang, Y. Constructing Stake Structured TiO_2-NTs/Sb-Doped SnO_2 Electrode Simultaneously with High Electrocatalytic and Photocatalytic Performance for Complete Mineralization of Refractory Aromatic Acid. *J. Phys. Chem. C* **2009**, *113*, 2375−2383.

DOI: 10.1021/am507826d
ACS Appl. Mater. Interfaces 2015, 7, 2745−2753